Kabir, R.; Albuerne, J.; Simon, P.F.W.; Filiz, V.; Abetz, C.; Boettcher, H.; Perlich, J.; Abetz, V.

Deformation and orientation behavior of polystyrene-b-polybutadiene-b-poly(methyl methacrylate) triblock terpolymers: Influence of polybutadiene microstructures and the molar masses

In: Polymer (2012) Elsevier

DOI: 10.1016/j.polymer.2012.11.075

Deformation and orientation behavior of polystyrene-*b*-polybutadiene-*b*-poly(methyl methacrylate) triblock terpolymers: Influence of polybutadiene microstructures and the molar masses

Rakibul Kabir[a,§], Julio Albuerne[a,&], Peter F. W. Simon[a$], Volkan Filiz[a], Clarissa Abetz[a], Heinrich Böttcher[a], Jan Perlich[b], Volker Abetz[a]*

[a]Institute of Polymer Research, Helmholtz-Zentrum Geesthacht, Max-Planck-Straße 1, 21502 Geesthacht, Germany

[b] HASYLAB, DESY, Notkestr. 85, D-22607 Hamburg, Germany

[§]*present address*: CAT Catalytic Center, ITMC, RWTH Aachen University, Worringerweg 1, 52074 Aachen, Germany

[$]*present address*: Faculty of Life Sciences, Rhein-Waal University of Applied Sciences, Marie-Curie-Straße 1, 47533 Kleve, Germany

[&]*present address*: BASF Polyurethanes GmbH, Elastogranstraße 60, 49448 Lemförde, Germany

*Corresponding author:

e-mail: volker.abetz@hzg.de

tel. +49 4152 87 2461

fax: +49 4152 87 2499

Abstract

Morphological changes caused by deformation and orientation of different domains of polystyrene-*b*-polybutadiene-*b*-poly(methyl methacrylate),SBM, triblock terpolymers were investigated using *in-situ* small angle X-ray scattering (SAXS), tensile testing, and transmission electron microscopy (TEM). Two sets of SBM triblock terpolymers with similar weight fractions of the three blocks were studied. The two sets differ in terms of their molecular weights. Each set contained two SBM differing in their polybutadiene isomers (1,2- and 1,4-B). Results showed that for 1,2-B based SBMs polybutadiene forms cylindrical domains which coalesce in the glassy lamellar matrix of the two glassy outer blocks whereas the lower molar mass 1,4-B based SBM forms mixed S/M and the higher one forms well segregated long range ordered lamellae. These morphological differences indicate that the deformation and the orientation behavior of the polymers' domains differ. In 1,2-B based SBMs yielding at high stresses was followed by a stress drop after the yield point. The other polymer type showed homogeneous deformation of the lamellar domains at their yield point. 2D-SAXS during deformation of the triblock terpolymers showed an anisotropic deformation pattern in the 1,2-B SBMs, whereas four point SAXS patterns were found for the 1,4-B SBMs. Further studies showed that the fragmented lamellar planes of the lower molar mass 1,2-SBM oriented randomly whereas the orientation of the lamellar planes of the higher molar mass 1,2-B SBM was parallel to the strain direction. The alignment of the lamellar planes of 1,4-B SBMs were randomly distributed in the unstretched state.

Keywords:

Block copolymer, deformation, orientation, polybutadiene microstructure

1 Introduction

Polymeric materials composed of different blocks show a broad variety of morphological patterns. The simplest and most widely studied block copolymers are AB diblock copolymers, where two building blocks of different nature are joined together by a covalent bond. The morphologies of AB diblock copolymers are mainly determined by one segmental interaction parameter, χ, the total degree of polymerization, N, and one independent composition variable like the volume fraction φ_A. Compared to AB diblock copolymers, ABC triblock terpolymers introduce more variables into the morphological behavior. The interplay of three segmental interaction parameters, χ_{AB}, χ_{BC}, χ_{AC}, the total degree of polymerization, N, and two independent composition variables, φ_A, and φ_B, respectively, result in a wide variety of complex morphologies in ABC triblock terpolymers.[1, 2]

The mechanical properties of block copolymers have been intensively investigated to explore suitable industrial applications. Deformation mechanisms of block copolymers differ from those of homopolymers because the microphase separated domains of block copolymers are too small in size for crazing to initiate.[3-6] The possibility to synthesize ternary block copolymers (mainly triblock terpolymers) has triggered the discovery of novel morphologies and opened new ways to control the mechanical properties as well as the deformation behavior.[7]

In the last few decades, the structure-property relationships and the deformation mechanisms of di- and tri-block copolymers based on thermoplastic elastomers (TPE) containing glassy and rubbery segments have been investigated.[3, 8-14] In general, TPEs are composed of two or more microphase-separated components. The most commonly used TPE is the binary triblock copolymer polystyrene-*b*-polybutadiene-*b*-polystyrene, SBS. Here, the rubbery B middle block is covalently linked to both the glassy S end blocks where the B chains are arranged in loops and bridges between the glassy domains (cf. Scheme 1). However, the B chains that form loops (i. e. both S end blocks are located in the *same* domain) hamper the elastomeric properties. The mechanical behavior also strongly depends on the morphological pattern and

microdomain orientation.[10] Changing the morphology of the rubbery B-domain from a lamellar to a cylindrical or a spherical pattern changes the mechanical behavior of the polymer from a thermoplastic elastomer to a high impact plastic.[7]

To circumvent the formation of the loops formed by the elastomeric middle block and therefore to improve the mechanical properties, one of the two S blocks can be replaced by another glassy-type polymer. For example, the use of a poly(methyl methacrylate), M-block leads to the ternary triblock TPE polystyrene-*b*-polybutadiene-*b*-poly(methyl methacrylate), SBM. As the glassy S and M phases are immiscible in that case, the elastomeric B chains are forced to form bridges (i.e. both end blocks are located in *different* domains) rather than loops, which enhances the mechanical properties of the polymer.[15]

(SCHEME 1)

Till now, only a limited number of publications addressing the deformation mechanism of SBMs during tensile testing have been published. Stadler and co-workers[16] demonstrated the deformation mechanism of SBM triblock terpolymers of symmetric and asymmetric type. For the symmetric type (both end blocks have similar weight fractions, resulting in lamellae (*ll)*, lamellar cylinder *(lc)* and lamellar sphere (*ls*) morphologies), the deformation mostly took place in the M phase. In the case of asymmetrically composed SBMs (having morphologies like cylinder at cylinder *(c_ac)* or cylinder in cylinder *(c_ic)*), a plastic deformation of the S matrix was reported. However, no additional information concerning the orientation of the different domains or the deformation pattern of the rubbery B domains was deduced from those results. Hence, the goal of our work is to interpret the deformation and orientation behavior of the SBM triblock terpolymers with a special focus on the polybutadiene middle block. Furthermore, the existence of two different structural isomers of the B block (i. e. 1,2-B and 1,4-B) must be considered as they cause a tremendous influence on the morphological as well as the mechanical properties.[17] To our knowledge, the influence of the microstructure of the B- domains on the deformation and orientation of lamellar domains during tensile test has not been addressed in the literature so far. In this paper we address the question of the influence of the microstructure of the rubbery

polybutadiene middle block on the morphological and deformation properties of SBM triblock terpolymers with approximately similar relative amounts of the three comonomers.

As many compositional variations are possible, we kept the relative amounts of the different blocks approximately equal, in order to compare the effects of the two B-isomers on the morphological deformation. Two pairs of the 1,2- and 1,4-SBMs were prepared with a lower and a higher molecular weight, respectively. The polymers were characterized by in-situ tensile test and 2D-SAXS experiments. Transmission electron microscopy (TEM) was performed on the specimens before and after tensile testing to analyze the morphological changes induced by large strains.

2 Experimental section

2.1 Materials

All SBM triblock termpolymers were synthesized on a 10g scale with varying block lengths and a narrow molar mass distribution by sequential anionic polymerization. Details of the experimental techniques and reaction conditions can be found elsewhere.[17, 18] The compositions and the molar masses of the SBMs investigated will be compiled according to a general formula ${}^{m}S_{x}B_{y}M_{z}{}^{n}$. Herein *m* represents the B's major type of isomers; *x*, *y*, *z* are the weight fractions of the respective blocks, and *n* is the number averaged molar mass of the polymer in kg/mol.

2.2 Sample preparation for tensile testing

To prepare solution cast films of a thickness of 350 to 400 µm, the polymers were dissolved in $CHCl_3$ and poured into Petri dishes. The solvent was allowed to evaporate slowly over 3-4 weeks at room temperature. Films were dried *in vacuo* at 30 °C for 2 days. The temperature was subsequently raised over a period of 24 hours to 100 °C, then again to 160 °C. The films were then cooled to room temperature.

2.2 Transmission Electron Microscopy (TEM)

The bulk morphology of SBM triblock terpolymers was studied by bright field TEM using an FEI Tecnai 20 operated at 200 kV. Thin sections (thickness 20-30 nm) were

cut at room temperature using a Leica Ultracut UCT Ultramicrotome equipped with a diamond knife. The thin films were stained by exposure to OsO_4 vapor for 1 to 3 minutes. A small piece of each sample was cut close to the fracture surface after tensile test. The orientation of the TEM samples related to the samples used for the stress-strain experiment was perpendicular to the tensile direction.

2.3 Small Angle X-ray Scattering (SAXS)

The bulk morphology was complementary studied by small angle X-ray scattering (SAXS). In-situ SAXS and stress-strain experiments were carried out at BW4 beamline of DORIS III, HASYLAB at DESY, Germany. The experiments were done at room temperature. 2D SAXS images were captured with a marCCD165 detector at different times during the stress-strain experiments. The sample – detector distance was set to 4 meters and a 1.38 Å X-ray wavelength was used. The data was analyzed with the help of the freeware software Fit2D[19]. In order to avoid misleading interpretations, a background image was taken after each experiment and was subtracted from the data. The distribution of the scattered intensity was plotted as a function of the azimuthal angles vs. intensity. Intensities at 90° and 270° correspond to the tensile direction which is referred to as meridional scattering, whereas the angles 0° and 180° correspond to equatorial scattering which is defined by the experimental set-up in a direction perpendicular to the stretching.

2.4 Stress-strain experiments

The stress-strain experiments were carried out on a “Zwick” model Z020, with a load cell of 0.5N. The measurements were done with a crosshead speed of 5 mm/min at ambient temperature according to the standard ASTM D882. The shapes of the samples were rectangular with an average dimension of 12 mm x 35 mm x 350 -400 µm.

2.5 Differential Scanning Calorimetry (DSC):

Differential scanning calorimetry (DSC) was performed using a Netzsch DSC Phoenix. The equipment was calibrated using indium and cyclohexane. Standard aluminium pans of 50 µL were used to encapsulate samples of 10 mg ± 1 mg. Dynamic heating and

cooling scans were performed under nitrogen atmosphere at heating rate 20 K min^{-1}. A second heating was used to evaluate the thermal transition of the polymer. The middle points of the transition curves were taken to determine the glass transition temperature, T_g.

3 Results and Discussion

The molecular compositions, molar masses, and the polybutadiene microstructure of two sets of SBM are given in Table 1. The absolute molar masses were calculated by a combination of GPC (absolute mass of the S precursor) and ^{1}H-NMR (weight fraction). To compare the influence of the two B-isomers the relative amount of the different blocks was kept constant. To further elucidate the effect of the overall chain length one set exhibiting lower and the second one with higher overall molar masses were investigated.

The polymers of set 1 exhibit a molar mass of approx. 55 kg/mol. In set 1 the polymer $^{1,2}S_{31}B_{31}M_{38}{}^{55}$ contains 90% of 1,2-B whereas in $^{1,4}S_{30}B_{29}M_{41}{}^{53}$ the content of 1,2-B is only 16%. Set 2 features molar masses in the range of 80-90 kg/mol. $^{1,2}S_{32}B_{31}M_{37}{}^{91}$ possesses 89% of 1,2-B whereas the 1,2-content is only 18% in case of $^{1,4}S_{34}B_{31}M_{35}{}^{80}$.

(TABLE 1)

Eight specimens of each polymer were tensile tested. The average values of the relevant mechanical properties and the standard deviation of the polymers are highlighted in Table 2. It seems that the B-microstructure has an important influence on the elastic modulus, the yield strength and the elongation at break of the terpolymers studied. The elastic modulus and the yield strength were higher in the case of the 1,2-B based SBMs, while the 1,4-B type terpolymers showed higher strain at break. The differences in the yield strength and the stress-strain trends of the 1,2- and 1,4-types SBMs clearly showed

plastic deformation in the 1,2-based SBMs and also in the 1,4-type with higher molar mass. The absence of a yield point in the case of the lower molar mass 1,4-SBM indicated a homogeneous deformation of the lamellar domains. Taking into account that the tensile tests were performed from cut films, the deviations of the presented results are remarkably good. The TEM images of the specimens at initial deformation during the tensile test are given in Figure 1. Interestingly, low molar mass $^{1,2}S_{31}B_{31}M_{38}^{55}$ shows a brittle behavior whereas a macroscopic localized shear yielding (i.e., necking) can be seen at higher molar mass $^{1,2}S_{32}B_{31}M_{37}^{91}$. As reported in the literature [19] [20] the presence of the B domains caused a homogeneous yielding in the glassy S lamellar phase of the styrene/butadiene based star block copolymer. In the present case probably the high molar mass 1,2-B domains did not fragment completely and dissipate the mechanical forces to the glassy domains. In the 1,4-B predominant polymers (i.e., Figure 1c and 1d) no crazing was observed. In the following sections the deformation behavior of the B microstructures are further discussed. The glass transition temperatures (T_g) were also listed in Table 3 for a better understanding of the influence of the B microstructure on the polymers' morphology.

Table 2

(Figure 1)

Table 3

3.1 Morphology of $^{1,2}S_{31}B_{31}M_{38}^{55}$ and $^{1,4}S_{30}B_{29}M_{41}^{53}$ before and after tensile test

3.1.1 Morphology of $^{1,2}S_{31}B_{31}M_{38}^{55}$

Figure 2a shows the TEM image of $^{1,2}S_{31}B_{31}M_{38}^{55}$ in the absence of strain. The S, B, and M domains can be distinguished from their color codes. The morphology features a pseudo-hexagonally cylindrical pattern (circle 1). A lamellar glassy phase with undulated B lamellae can also be recognized (circle 2). The S domains are attached to the B ones and the M domains form a continuous phase surrounding the S and B domains.

(FIGURE 2)

The morphology after applying a strain of 100% is shown in Figure 2b where two different areas of the deformation patterns are presented (cf. circle 3 and 4). Circle 3 shows a zig-zag pattern of lamellar domains resembling a chevron-like morphology. The formation of the chevron-like morphology strongly resembles Ref [21, 22] where the deformation of lamellar SBS block copolymers was discussed. In analogy to their results we suppose that the chevron-like morphology in $^{1,2}S_{31}B_{31}M_{38}^{55}$ is formed if the stretching direction is perpendicular to the lamellar domains as indicated by the arrow in the TEM micrograph. Its evolution begins beyond the yield point attributed to fragmented lamellae. These fragmented domains can now orient more easily with the flexible B domains resulting in a zig-zag pattern as sketched in Figure 2c.

A schematic sketch of the deformation in circle 4 of Figure 2b is given in Figure 2d. The TEM image supports the hypothesis that the pseudo-hexagonally arranged B domains are elongated during stretching perpendicular to the cylindrical domains. Upon further stretching, four B cylinders are further deformed until they become linked with their ends. Finally, the extended S domain encloses the adjacent B domains (cf. circle 4). Odell and Keller[11] found an analogous morphology in an SBS triblock copolymer where hexagonally arrayed S cylinders were embedded in a rubbery B matrix. Application of a strain parallel to the cylinders resulted in stress-strain curves featuring a yield behavior at 3% strain. Even at small strains the yielded material became more compliant, potentially caused by the breakage and reformation of the cylinders. For SB

diblock copolymers Argon *et al.*[23] proposed a two-step craze growth mechanism with hexagonally packed B cylinders embedded in the S matrix. First, the material was elastically deformed up to a critical stress. When this critical stress was reached, cavitations occurred within the domains, leading to necking formation of the S matrix. In the case of the $^{1,2}S_{31}B_{31}M_{38}{}^{55}$, the evidence of the different domains orientations and the whitening of the films when the strain reaches 10% lead to the conclusion that crazes occurs in this sample, probably after the formation of microvoids. Unfortunately, the craze formation could not be followed by TEM, which might be due to the preparation of the samples for microscopy. In this study, the samples were taken after the strain-stress experiments were performed. The time between the strain-stress experiment and the preparation of the sample for the TEM experiments might has led to relaxation of the terpolymer and the disappearance of any evidence of crazing.

3.1.2 Morphology of $^{1,4}S_{30}B_{29}M_{41}{}^{53}$

Before stretching the specimen of $^{1,4}S_{30}B_{29}M_{41}{}^{53}$ (Figure 3a) shows a well segregated lamellar pattern with large microdomains. Though the contrast does not allow the differentiation between the S and M domains, a single T_g at 123.1°C lead us to conclude that these two glassy blocks form a mixed domain. (see Table 3). When the specimen is elongated up to 100% (Figure 3b) with the strain perpendicular to the lamellar direction (indicated by the white arrow), only minor distortions of a wavy pattern-type are observed in the B domains due to the high flexibility of the 1,4-B block. By increasing the strain up to 300%, the B lamellae become very wavy but still the lamellar domains can clearly be identified and they are not completely distorted. Stress hardening due to the entanglement of the B domains has very likely occurred at this stage. To monitor the deformation of the domains, the stress-strain experiments for both polymers ($^{1,2}S_{31}B_{31}M_{38}{}^{55}$ and $^{1,4}S_{30}B_{29}M_{41}{}^{53}$) were compared and are discussed in the following section.

(FIGURE 3)

3.2 Stress-strain behavior and deformation of morphology for low molar mass polymers $^{1,2}S_{31}B_{31}M_{38}{}^{55}$ and $^{1,4}S_{30}B_{29}M_{41}{}^{53}$

A tensile testing series is given in Figure 4. A magnification view of the stress-strain curves up to 50% strain is also shown. The elastic modulus of the terpolymer $^{1,2}S_{31}B_{31}M_{38}^{55}$ is found to be approximately two times higher than in the case of the $^{1,4}S_{30}B_{29}M_{41}^{53}$. Unfortunately, no tensile strength at yield could be estimated in the case of $^{1,4}S_{30}B_{29}M_{41}^{53}$ but, a qualitative comparison with the $^{1,2}S_{31}B_{31}M_{38}^{55}$ shows that before the start of the irreversible deformation of the terpolymer takes place, the tensile strength for the 1,2-B type terpolymer is also approximate two times higher. On the contrary, the strain at break for the polymer $^{1,2}S_{31}B_{31}M_{38}^{55}$ lays below 120%, while in the case of the $^{1,4}S_{30}B_{29}M_{41}^{53}$ exceeds this value, in some cases up to 700%.

For $^{1,2}S_{31}B_{31}M_{38}^{55}$ a sharp yield drop occurs due to the plastic deformation of the glassy domains which was also observed as a macroscopic necking associated with the appearance of microvoids. After the yield point, the stress level increased slowly, but due to the lack of network formation of the short and discontinuous B domains of this polymer (c.f. Figure 2a) the sample break occurred, regularly, below 100% strain.[21, 24]

(FIGURE 4)

For $^{1,4}S_{30}B_{29}M_{41}^{53}$ an increase in tensile strength occurred just after yielding (strain hardening), with a moderate neck formation. It can be speculated that for two adjacent continuous phases with highly different mechanical properties (in this case, glassy S or M, respectively, and rubbery B), most of the mechanical forces are absorbed in the elastic domains without distorting the glassy ones. That means the moderate necking occurs because of an incomplete distortion of the hard S and M domains. Yamaoka *et al*.[10] also reported this kind of moderate necking at the yield point followed by necking which resulted in a chevron-like morphology. The occurrence of strain hardening at higher elongation occurred by network hardening of the continuous 1,4-B chain.[25] Such stress-strain behavior with a low yield point is a typical feature of a rubbery material.

3.3 In-situ combination of 2D-SAXS and tensile testing for low molar mass SBM

3.3.1 In-situ tensile test-SAXS experiment of $^{1,2}S_{31}B_{31}M_{38}^{55}$

In-situ 2D-SAXS tensile testing results of $^{1,2}S_{31}B_{31}M_{38}^{55}$ show the deformation behavior (Figure 5) depicting a stress-strain plot as well as 2D-SAXS images recorded at strains of 0%, 7%, 31%, and 53% strain, respectively.

(FIGURE 5)

From the 2D-SAXS images intense scattering at small q values was observed for $^{1,2}S_{31}B_{31}M_{38}^{55}$. This scattering occurs under fragmentation of the lamellar domains during tensile deformation. At the initial stage ($\varepsilon = 0\%$) an isotropic two ring pattern is found due to the random orientation of the domains. Close to the yield point ($\varepsilon = 7\%$), the symmetrical ring pattern develops into an ellipse, with the longer axis being oriented along the equator. A yield drop occurs when the glassy domains are distorted; hence the tensile stress is transferred over the rubbery domains causing a plastic to rubbery transition at this stage. At 31% elongation, the outer ring (2^{nd} order scattering) diffuses completely while the inner ring (1^{st} order scattering) elongates to the equator direction. Most probably the rubbery domains break down at this stage and are arranged randomly. Finally, at the elongation of 53% the anisotropic scattering of the inner ring further elongates into the equatorial direction. This might indicate that the rubbery domains are now highly extended. The domain sizes of B changed from 10 ± 1 nm ($\varepsilon = 0\%$) to 5 ± 2 nm at maximum strain as calculated from the TEM micrographs.

(FIGURE 6)

The preferential orientation of the domains and their evolutions are further investigated by plotting the first order scattering as a function of the azimuthal angle. The azimuthal plot shows a continuous shift of the scattering intensity with the increase of the strain (see Figure 6a). This means that the evolution of orientation of the microdomains depends on the strain. At 0% strain, no dependence of the intensities profile on the azimuthal angles can be found indicating the presence of randomly oriented cylindrical domains. When the strain reaches 7%, two scattering maximum can be recognized, one

located between 0° and 20°, and a second between 155° and 200°. At a strain of 31% the maxima scattering are located at φ = 0° and 180°. The intensity of these maxima is relative lower than at 7% of deformation. This evolution continues at 53% of strain, indicating a change on the scattering of the domains from the meridional to equatorial axis. The corresponding change of the scattering of the domains during the elongation can be deduced from Figure 6b, where the scattering intensity *vs.* the scattering vector *q* for different strains is shown. The 1-D SAXS was taken at φ = 180°. The first two peaks are continuously increasing up to 53% of strain. They correspond to the central diffusion. The two sharp peaks at 0.14 nm^{-1} and 0.24 nm^{-1} appear at 0% of strain, which have a relative position of $1:3^{1/2}$ indicating hexagonally packed cylinders. The intensity of the peaks reduces and at the same time the width of the peaks increases at 7% strain indicating the decrease of the correlation length of the plane perpendicular to the strain direction. The peak intensities further decrease for 31% strain and for 53% no distinct peaks can be observed.

This might be due to the complete disintegration of the microdomains or because the distances within microdomains are outside the detection limits in the experimental setup used.

3.3.2 In-situ tensile test-SAXS experiment of $^{1,4}S_{30}B_{29}M_{41}{}^{53}$

The 2D-SAXS patterns at different strain values are shown in Figure 7 for the terpolymer $^{1,4}S_{30}B_{29}M_{41}{}^{53}$. Compared to $^{1,2}S_{31}B_{31}M_{38}{}^{55}$, the fragmentation of the microdomains of $^{1,4}S_{30}B_{29}M_{41}{}^{53}$ seem to occurs less which can also be recognized from the specimen pictures in Figure 1a,c where no crack in the specimen is seen. At 0 % strain, two scattering rings can be identified in the 2D-SAXS pattern, one seemly close to the beam stop. At the first stages of deformation, the terpolymer scatters preferentially along the equatorial direction that elongates up to 100 % strain. However, a scattering shift to the equatorial direction was identified which means the fragmented domains start to orientsalong the strain direction. Close to the yield point (ε ≈16%) the meridional scattering maximum disappears. This might indicate that almost all microdomains which originally were oriented perpendicular to the stretching direction

have changed their orientation. At this stage a four point pattern starts to appear which is well developed at ε = 70%. In this regime, the equatorial 2D-SAXS pattern changes to a pattern characteristic of a grain structure in which the lamellar surfaces are inclined with respect to the strain direction. At strain values up to 300%, the scattering lobes tend to elongate parallel to the equator. Here, the lamellar domains become strongly undulated as shown in the TEM micrographs in Figure 3c.

Also note that the domain spacing parallel to the strain direction increases with the elongation. When the strain has reached 400%, the spacing becomes broader and the lobes come closer to each other. It seems that the complete fragmentation of the glassy domains has not occurred at this stage; an observation also supported by Figure 7 as the four point lobes can still be recognized even at strains exceeding 400%. Different from this behaviour, at comparable strains the fragments of the SBS's glassy phase are randomly dispersed in the rubbery B-matrix resulting in the disappearance of distinct scattering peaks.[10] Hence, the SBM system shows higher elastomeric properties compared to its SBS analogue as the fraction of B chains in SBM are bridging the two end domains.[15]

(FIGURE 7)

As we are interested in the deformation evolution of the 1,2- and 1,4-B domains, the azimuthal plot of the 1st order reflection which was splitted into four lobes was interpreted with changes of the azimuthal angle for different elongation ratios (see Figure 8a). In absence of strain the scattering intensity is independent of the azimuthal angle. At 10% strain, four scattering maxima appear at ϕ =27°, 157°, 203°, and 334°, respectively. For increasing strains the four maxima become more distinct and shift to an azimuthal angle, ϕ = 10°, 170°, 190°, and 350° indicating an evolution of the orientation of the planes related to the strain direction.

(FIGURE 8)

Figure 8b shows the 1D-SAXS patterns corresponding to the one dimensional cut of the 2D-SAXS patterns at 90° for different strains. Higher order reflections are to be

expected outside the measurement window and therefore cannot be discussed in terms of the symmetry of the morphology. When the strain reaches 10%, the intensity decreases and the maximum position shifts to higher *q* values. At 100% strain, the intensity further decreases but the peak's width broadens. Finally, at ε = 400%, the peak is barely visible. This trend can be attributed to an increasing disorder in the distance of the orientation plane and to a reorientation of the microdomains.[8] The change of the domain lengths during stretching and of the long range order of SBMB can also be deduced from the TEM micrographs and SAXS reflection peaks, cf. Table 4. At 0% strain both the glassy lamellar domains exceed the dimensions of the B ones. At 300 % of deformation, the domain's size decreases. This effect is most obvious in the case of the B (from 7 nm to 5 nm), demonstrating the rubbery character of this domain compared to the glassy S and M ones. The long period corresponding to the SAXS first order reflection at q = 0.23 nm^{-1} was calculated 27.31 nm at ε = 0 % which decreases to 25.12 nm at 300 % strain. The values are comparable to the TEM results (e.g., Table 4).

(TABLE 4)

3.4 Morphology of $^{1,2}S_{32}B_{31}M_{37}{}^{91}$ and $^{1,4}S_{34}B_{31}M_{35}{}^{80}$ before and after tensile test

3.4.1 Morphology of $^{1,2}S_{32}B_{31}M_{37}{}^{91}$

The TEM images of the $^{1,2}S_{32}B_{31}M_{37}{}^{91}$ sample before and after the tensile test are shown in Figure 9. The unstretched sample exhibits a very well ordered array of S and M lamellae (Figure 9a). The three T_g's of the different blocks (i.e., Table 3) also resemble a good segregation of the different blocks. However, the B lamellar domains are discontinuous and in some parts of the micrograph a cylindrical pattern (cf. magnification of the TEM micrograph in Figure 9a) can be found.

(FIGURE 9)

The deformation of the morphology at 300% strain is highlighted by a magnified view of the B domains with extra contrast for clarity. Two deformation patterns can be

identified in the image: (i) a screw-type pattern as shown in the circled area 3. Here, no deformation of the adjacent S and M is observed, only the B cylinders are oriented and twisted in a screw-type pattern, (ii) a wavy pattern of continuous B lamellae (see circle 2) embedded in the deformed glassy lamellar domains of S and M.

3.4.2 Morphology of $^{1,4}S_{34}B_{31}M_{35}^{80}$

Figure 10a shows the TEM images of $^{1,4}S_{34}B_{31}M_{35}^{80}$, where a well segregated lamellar morphology with continuous lamellar domains is observed. The effect of 300% strain on the morphology is shown in Figure 10b. Two types of deformation are observed. When the strain direction is perpendicular to the lamellar orientation, a chevron-like morphology is obtained, which is formed by the combined mechanisms of shearing, kinking, destruction, and reorientation of the B lamellae accompanied by fragmentation of the S and M hard phases.[8] Strain hardening at larger elongation leads to very wavy and sometimes distorted B domains (cf. circle 2). In some areas the domains are even disconnected from long lamellar ones.

(FIGURE 10)

3.5 Stress-strain behavior and deformation of morphology for high molar mass $^{1,2}S_{32}B_{31}M_{37}^{91}$ and $^{1,4}S_{34}B_{31}M_{35}^{80}$

Eight specimens of each polymer were tested and the resulting stress-strain curves with a magnification for low strains ($\varepsilon \leq 50$ %) are plotted in Figure 11. In both polymers stress whitening was seen, however, no cracks were formed. This could be due to the high molar mass of the B domains, which enhance the tensile loading of the terpolymers. In the stress-strain curve of $^{1,2}S_{32}B_{31}M_{37}^{91}$ the plots show a maximum strain at break between 300% and 400%. On the other hand, for $^{1,4}S_{34}B_{31}M_{35}^{80}$ the highest strains at break are observed at 600% to 700%. The E-moduli and the tensile strength at yield of $^{1,2}S_{32}B_{31}M_{37}^{91}$, as well as in the low molecular weight case, are higher than the $^{1,4}S_{34}B_{31}M_{35}^{80}$. The highest tensile strength at yield for $^{1,2}S_{32}B_{31}M_{37}^{91}$ was observed at approximately 27 MPa, whereas for $^{1,4}S_{34}B_{31}M_{35}^{80}$ the values are around 17 MPa. The higher tensile strength at yield in $^{1,2}S_{32}B_{31}M_{37}^{91}$ is caused by the higher content of less-flexible 1,2-B. The sample $^{1,2}S_{32}B_{31}M_{37}^{91}$ also forms a neck, similar to its lower

molecular weight counterpart. After the yielding, strain softening is followed by strain hardening. The large elongation at break is supposedly associated with a fragmentation process of the glassy lamellae and a more pronounced tendency of strain hardening.[20] However, for $^{1,4}S_{34}B_{31}M_{35}^{80}$ the stress tends to increase monotonically until the specimen breaks. The strain hardening seems to be more prominent for the 1,2-B-isomer. This observation may be caused by a higher tendency of the 1,4-B isomer to form network hardening at higher elongation.[25]

(FIGURE 11)

3.6 In-situ combination of SAXS and tensile testing for high molar mass SBM

3.6.1 In-situ combination of SAXS and tensile testing of $^{1,2}S_{32}B_{31}M_{37}^{91}$

The stress-strain curve together with 2D-SAXS patterns at given strains of $^{1,2}S_{32}B_{31}M_{37}^{91}$ is shown in Figure 12.

(FIGURE 12)

The evolution of the domain's fragmentation and the scattering intensity at different strain values is similar to the low molar mass analogue (for comparison, see Figure 5). In $^{1,2}S_{32}B_{31}M_{37}^{91}$ three scattering rings are recognized. The evolution of the inner scattering ring with the strain cannot be follow, because it is too close to the beam stop. Interpretation of this scattering could lead to misunderstanding. For this reason, the scattering close to the beam stop was not considered. Hence, the second scattering rings were considered for the deformation and orientation analysis of the fragmented domains. At a yield point of 6% strain the meridional SAXS maximum changes to an equatorial one which indicates the deformation of the glassy domains. When the strain has reached 18%, the second scattering ring becomes almost undetectable. Obviously, strains between 6 % and 18 % cause necking of the glassy lamellae accompanied by shearing in the rubbery phase, i.e. the so-called 'plastic to rubbery transition' occurs.[9, 26] At higher elongations, e.g. at nearly 400%, the equatorial 2D-SAXS maximum can still be detected but its close vicinity to the meridional one and the beam stop does not allow an evaluation.

The observation that during the deformation process the scattering intensities were redistributed to the equatorial SAXS maximum, suggests that orientation and disorientation processes of the domains occur along the strain direction. This type of anisotropy scattering is well known for semicrystalline polymers[20] and samples with a cylindrical morphology for both large and small strains[22] resulting from a different orientation of lamellae.[20, 22] Interestingly, the redistribution was also reported for a rubber-modified glassy amorphous polymer blend[27] where the redistribution of the scattering intensity was explained by the presence of the effect of shear yielding and the absence of cavitations.

The thickness of the lamellae also decreases during homogenous deformation (cf. Table 5). The changes of the domain sizes (calculated from TEM images) show that at 0% strain, the M domain is broader than the other two where the B domain being the narrowest one. At a strain of 300%, all domains become narrower. The effect is not emphasized in the case of the S and M domains, but, it is much more pronounced for the B domains (from 14 nm to 9 nm). The distance of the interdomain planes increases from 78 to 86 nm during stretching up to 300% which was calculated from the SAXS 2nd order reflection peak.

(TABLE 5)

The reorientation of the fragmented domains was further analyzed by plotting the azimuthal angle vs. strain. The scattering at strain ε = 0% of q = 0.16 nm^{-1}was considered (see Figure 13). The intensity of the 2nd reflection peak remains almost constant for strains up to 6% indicating the absence of plastic deformations in this range. However, for higher strains an intensity maximum develops at an angle of 0° and 180° (Figure 13a). The peak narrows at higher elongations (e. g. 400%), indicating that the domains are oriented parallel to the stretching direction. Figure 13b shows the relation between the intensities and the scattering vector, q for the different strains. When increasing the strain up to 6%, the intensity at q = 0.16 nm^{-1}starts to diminish, which is in accordance with the disappearance of the meridional SAXS maximum in Figure 12. At 18% strain that peak has completely disappeared, however, at the same time, the first order peak at q =0.08 nm^{-1} is continuously shifting to lower q-values with

increasing strains (i.e. 31% to 400%) which is due to the orientation of the fragmented domains .

(FIGURE 13)

3.6.2 In-situ combination of SAXS and tensile testing of $^{1,4}S_{34}B_{31}M_{35}^{80}$

In the case of $^{1,4}S_{34}B_{31}M_{35}^{80}$ the sequence of morphological deformations with increasing strain is summarized in the SAXS patterns of Figure 14. Intially at 6% strain the scattering located in the meridional 2D-SAXS patterns diminish, which might be an indication of the plastic deformation of the glassy domains. At ε = 23% the re-orientation of the domain into the strain direction can be concluded as the four point lobes of the equatorial SAXS appear. Though in $^{1,4}S_{30}B_{29}M_{41}^{53}$ the four lobes scattering peaks exist above 600% strain, in $^{1,4}S_{34}B_{31}M_{35}^{80}$ they start to diffuse at 39% strain. At 156% the four lobes are completely diffused as can be seen in Figure 14. At this stage, a transformation of the domains from a chevron-like pattern to a random one takes place. Afterwards the tendency of the scattering increases anisotropically to the equatorial direction upto 469% strain. As this scattering pattern appears at higher strain values for $^{1,4}S_{34}B_{31}M_{35}^{80}$, a difference on the development of the scattering intensity as a function of the azimuthal angle is also observed (see Figure 15)

.

(FIGURE 14)

The orientation of the diffusion intensity can further be investigated by correlating the azimuthal angle as shown in Figure 15a. Like $^{1,2}S_{32}B_{31}M_{37}^{91}$, the highest intensity maximum develops at an angle of 0° and 180°. The scattering intensity at the meridional direction (at 90° and 270°) increases up to 219% strain. However, the diffraction peaks of the four lobes at 157° and 203° are only slightly visible at 6% strain which diffuse and reorient further to the tensile direction. Finally, at 469% strain the scattering intensity increases only to the equatorial direction but the intensity maxima at ϕ = 90° and ϕ = 270° almost disappear probably due to random orientation of the domains. Only

the intensity of the 0° and 180° peak continuously increases at this stage which is mainly caused by the deformation of the rubbery domains along the strain direction. The plot of the intensity versus *q* (Figure 15b) also highlights the changes of the orientation of the planes at different strain. The 1-D SAXS was taken at φ = 180°. The first two scatterings at 0.05 $nm^{-1}$and 0.07 nm^{-1} are too close to the beam stop and cannot be resolved with the increase in the strain values. Correlation between the scattering peaks corroborates that the lamellar morphology observed by TEM. At higher strain values the changes of the interdomain planes were estimated from the TEM image of Figure 10 and listed in Table 6. At 0% strain, the M domain is broader than the S and B ones with B being the narrowest. Application of strain leads to a reduction in domain sizes of about 4 — 5 nm. The SBMB periodicity calculated from TEM micrograph (cf. Figure 10a) and SAXS reflection peak (Figure 15b) becomes narrow at 300% strain.

(FIGURE 15)

(TABLE 6)

3.7 Orientation behavior of 1,2- and 1,4- SBM morphology

The orientation of uniaxial systems with respect to the reference direction (parallel to the symmetry axis of the system) can be expressed by Legendre polynomials. The second order Legendre polynomial, P_2 (orientation parameter), of this distribution function is the most often used parameter to describe the state of orientation in such a system. It can be obtained by integration of the scattering intensity $I_q(\varphi)$ as a function of azimuthal angle φ within the interval of φ = 0° to 360°.[28] P_2 is expressed as

$$p_2 = \frac{3 < cos^2\varphi > -1}{2}$$

where:

$$< \cos^2\varphi > = \frac{\int_0^{2\pi} d\varphi \, (I_q(\varphi) cos^2\varphi |sin\varphi|)}{\int_0^{2\pi} d\varphi \, (I_q(\varphi) |sin\varphi|)}$$

In the SAXS measurements on lamellar stacks the normal of the lamellae is giving the orientation of the scattered intensities. This means that for a uniaxial system with all lamellae being oriented perpendicular to the reference direction, P_2 will reach its maximum value of 1, indicating a perfect alignment. If the lamellae are oriented uniaxially parallel to the reference direction, then their normals will be homogeneously distributed in all perpendicular directions with respect to the reference direction, leading to the minimum value of P_2, which is -0.5. A random distribution of the lamellar stacks will lead to an isotropic situation with $P_2 = 0$.

For the investigated SBMs the plot of the orientation factor (P_2) versus the strain is given in Figure 16. The integration of the scattering profiles was performed for the interval 90° <φ< 270° close to the diffusion intensity in order to obtain actual deformation information of the domains. From that plot the orientation behavior of the copolymer domains during the elongation process can be deduced.

(FIGURE 16)

Unfortunately, only a very limited number of orientation factors (P_2) were obtained for $^{1,2}S_{31}B_{31}M_{38}{}^{55}$ all being very close to zero. As observed in the 2D-SAXS images, a random orientation of the fragmented domains was speculated. As in this polymer the domains are rather short and consist of the glassy S and M blocks, it is assumed that after the yield point the domains were fragmented and reached to their high stretching limit. For the high molar mass $^{1,2}S_{32}B_{31}M_{37}{}^{91}$ a different orientation behavior is observed. The orientation factor reaches -0.22 at the first deformation stage which indicates the alignment of the lamellae planes is more parallel to the stretching direction, i. e. normal are they more perpendicular to the chain axis. With a further increase of the strain up to 300% the lamellar domains continue to orient to the strain direction which is also highlighted in Figure 9b where the B phases turned into a wavy pattern in the stretching direction.

In the case of $^{1,4}S_{30}B_{29}M_{41}{}^{53}$, the P_2 value reaches -0.10 at the first stage of deformation and then slowly increases to -0.02 at higher strain. Again for the high molar mass $^{1,4}S_{34}B_{31}M_{35}{}^{80}$, the P_2 value is -0.06 and remains constant even for 400% strain. The maximum orientation reached by the low molar mass 1,4-B sample is double of the

value obtained for the high molar mass 1,4-B, which would be related with the ability of the soft block to facilitate the orientation of the lamellar hard block. It could be that the low molar mass 1,4-B has reached its chains stretching limits and hence the one of the whole block copolymer. In the case of the high molar mass variation may be the 1,4-B has not reached the limits of elongation and simply acts as a "plasticizer" of the hard domains. For this reason the lamellar stacks are probably randomly distributed. The corroborating TEM images in Figure 10b showed that the lamellar structure is not completely disrupted after 300% of deformation of the 1,4-B.

4 Summary

The effect of deformation on the morphology and the stress-strain behavior for two sets of SBMs was discussed. These differ in their 1,2-B to 1,4-B ratios and their total molar masses. In the case of 1,2-SBM, a co-existing lamellar and cylindrical morphology of B block was observed for both the low and high molar mass SBMs. However, in both 1,4-SBMs, only well segregated lamellar patterns were found.

Polymer $^{1,2}S_{31}B_{31}M_{38}^{55}$ exhibits a high yield stress followed by a stress drop after the yield point with macroscopic necking caused by the continuous M phase. In contrast, a typical rubbery behavior is found for $^{1,4}S_{30}B_{29}M_{41}^{53}$ which is dominated by its continuous B lamellar phase. The other two high molar mass SBMs show an intermediate mechanical behavior within these two extremes. $^{1,2}S_{32}B_{31}M_{37}^{91}$ exhibits a high yield drop at low strains where the B phase in the lamellar structure is no longer continuous, but alternates with S phases. Compared to this sample, its 1,4-B analogue shows a moderate yield drop at low strains and higher stress hardening at high strains.

The orientation of the fragmented domains was assessed with respect to the orientation parameter (P_2). In the case of the high molar mass 1,2-SBM ($^{1,2}S_{32}B_{31}M_{37}^{91}$), the orientation of the lamellar planes is mostly parallel to the strain direction. The orientation factor of $^{1,2}S_{31}B_{31}M_{38}^{55}$ cannot be evaluated due to the fully fragmentation domains a finding which is also supported by the brittle behavior in $^{1,2}S_{31}B_{31}M_{38}^{55}$. For SBMs containing a higher 1,4-B content, the lamellae change rapidly into a random domain orientation. In high molar masses analogue, the orientation is slightly parallel to the strain direction at initial stages but for higher strains a random orientation develops.

These results demonstrate that the microstructure of the B block and the molecular weight has an important influence on the mechanical behavior of the terpolymers. In the first case, the 1,2-B blocks tends to reach a maximum state of deformation and then the strain is transferred to the whole microdomains, increasing the orientation factor of the terpolymer. On the contrary, the lower T_g or the elasticity of the 1,4-B chains might tolerate the mechanical stress, leading to random orientation of the glassy domains. This study shows the influence of the nature of the rubbery centre block in thermoplastic ABC triblock terpolymers on their stress-strain behaviour.

Acknowledgements:

The authors thank Brigitte Lademann, Maren Brinkmann, Silvio Neumann, and Dr. Thomas Emmler for their support in anionic polymerization, GPC, DSC, and 1H-NMR spectroscopy, respectively. A part of this work was financially supported by the ESF Eurocores Programme SONS2 through the collaborative project “Complexity Across Length-Scales in Soft Matter (SCALES)”.

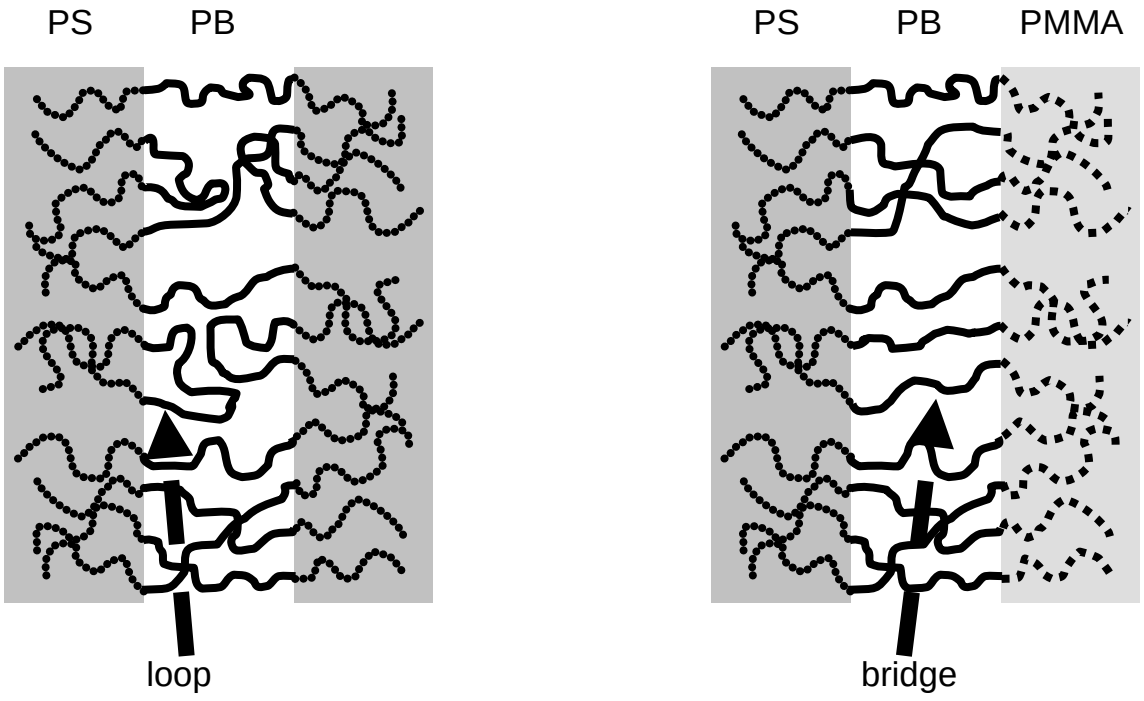

Scheme 1: *Sketch of the loop and bridge formation of the polybutadiene middle block in PS-b-PB-b-PS (SBS) (left) and PS-b-PB-b-PMMA (SBM) (right) systems*

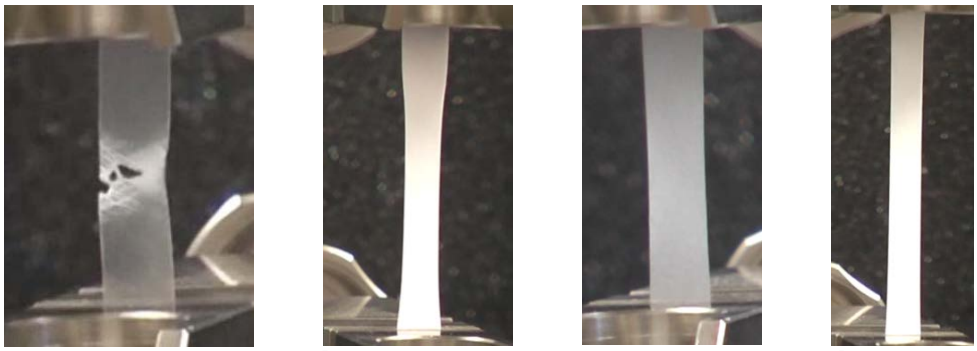

Figure 1: *Initial deformations of the specimens during tensile testing. The deformation patterns are a)crazing in* $^{1,2}S_{31}B_{31}M_{38}^{55}$*, b)necking and stress whitening in* $^{1,2}S_{32}B_{31}M_{37}^{91}$*, c) moderate necking and no crazing in* $^{1,4}S_{30}B_{29}M_{41}^{53}$*, and d) stress whitening in* $^{1,4}S_{34}B_{31}M_{35}^{80}$*.*

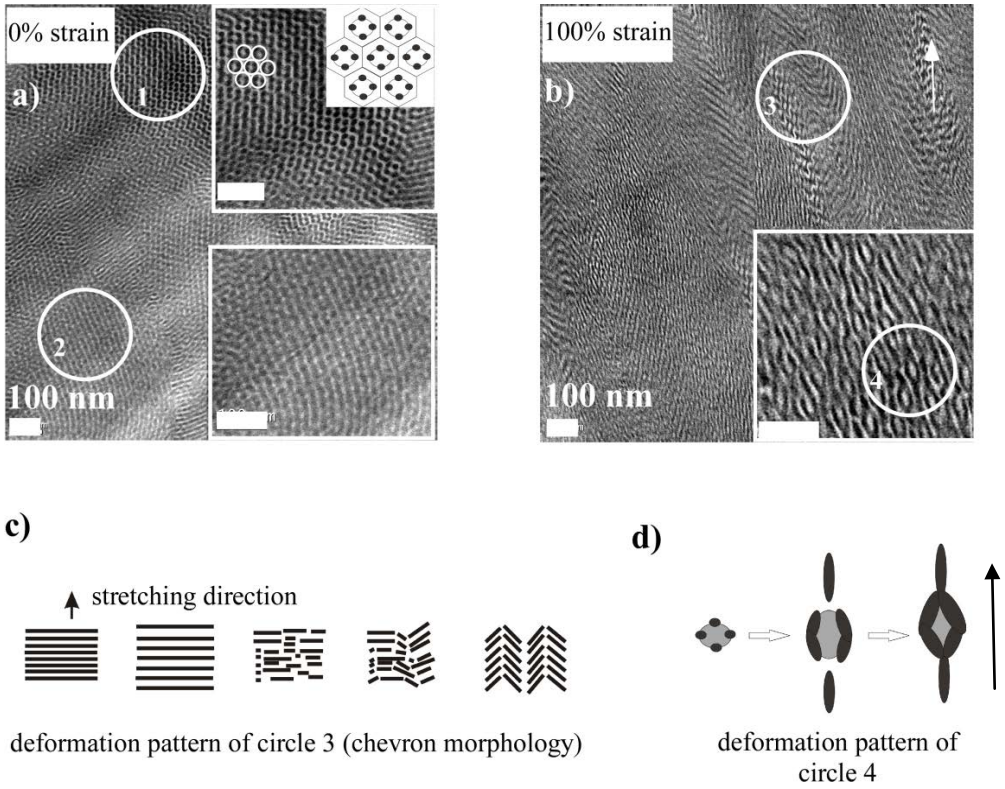

Figure 2: *TEM micrographs of* $^{1,2}S_{31}B_{31}M_{38}^{55}$ *stained with* OsO_4 *(S = gray, B = black, M = white). White scale bars indicate 100 nm.*

a): ε = 0 %.Circle 1:hexagonally arrayed B cylinders (cf. sketch at the right corner). Circle 2: lamellar area with undulated B lamellae.

b):ε = 100 %:white arrow indicates stretching direction. Circle 3: zig-zag pattern. Circle 4: deformation of the B cylinders.

c): sketch of the evolution of the deformation of a zig-zag pattern when stretching is perpendicular to the lamellar direction.

d): sketch of the evolution of the deformation pattern of cylindrical B domains from the surface view (cf. circle 4), stretching is perpendicular to the cylinders indicated by the arrow.

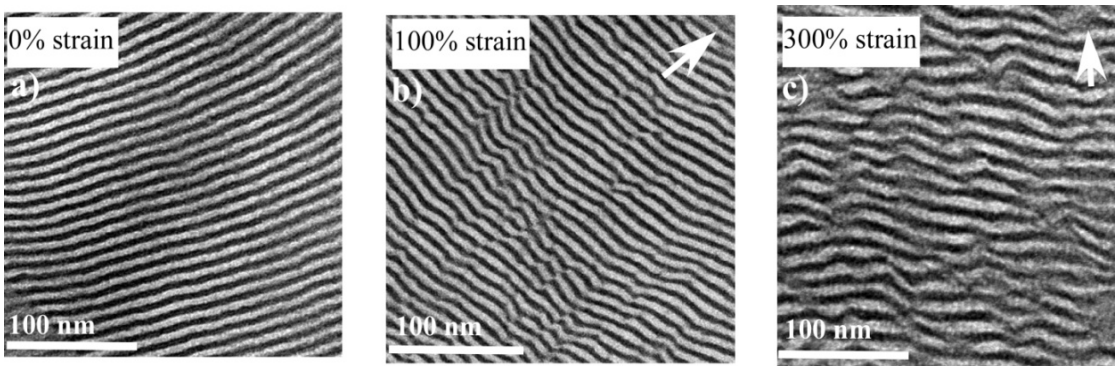

Figure 3: *TEM micrographs of* $^{1,4}S_{30}B_{29}M_{41}^{53}$ *stained with* OsO_4 *(color code: S/M mixed lamellae= gray, B = black) at a)ε = 0%, b)ε = 100%, and c)ε = 300% strain (white arrow indicates the stretching direction). Wavy B domains can be observed at 100% strain while some distorted B lamellae appear at ε = 300%*

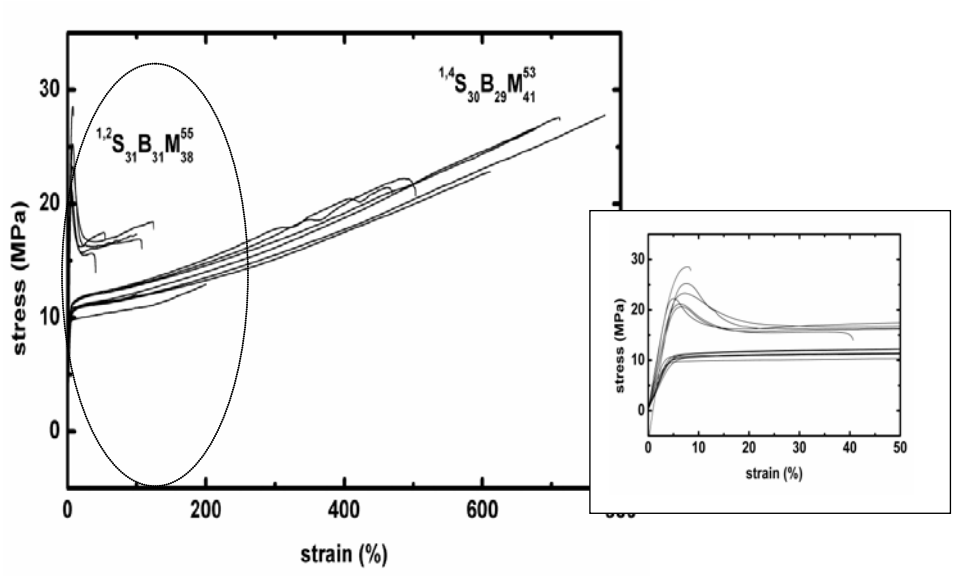

Figure 4: *Stress-strain curves of several specimens of* $^{1,2}S_{31}B_{31}M_{38}^{55}$ *and* $^{1,4}S_{30}B_{29}M_{41}^{53}$. *Magnification for strains ε< 50 % are shown in the inset*

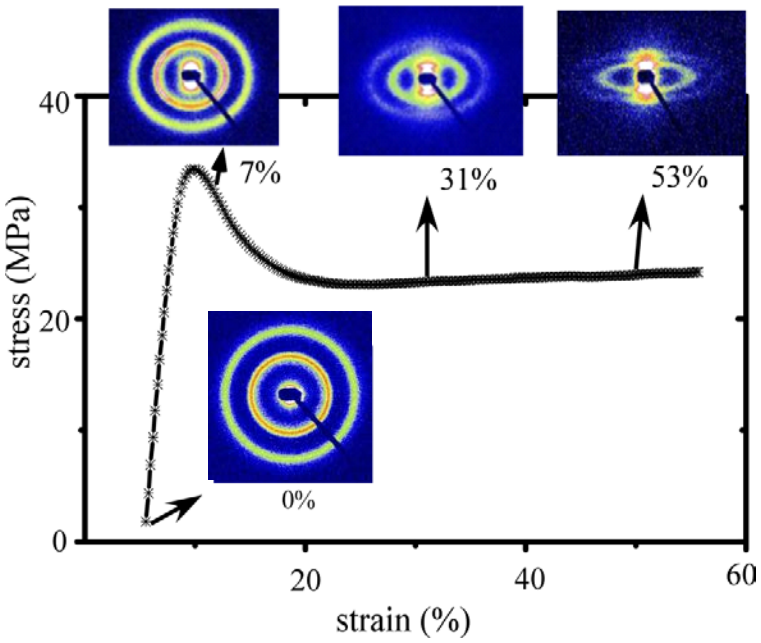

Figure 5: *Results of the combination of SAXS and tensile testing for* $^{1,2}S_{31}B_{31}M_{38}^{55}$. *Stress-strain diagram with the 2D-SAXS patterns obtained at strain of ε = 0%, ε =7%, ε =31%, and ε = 53%*

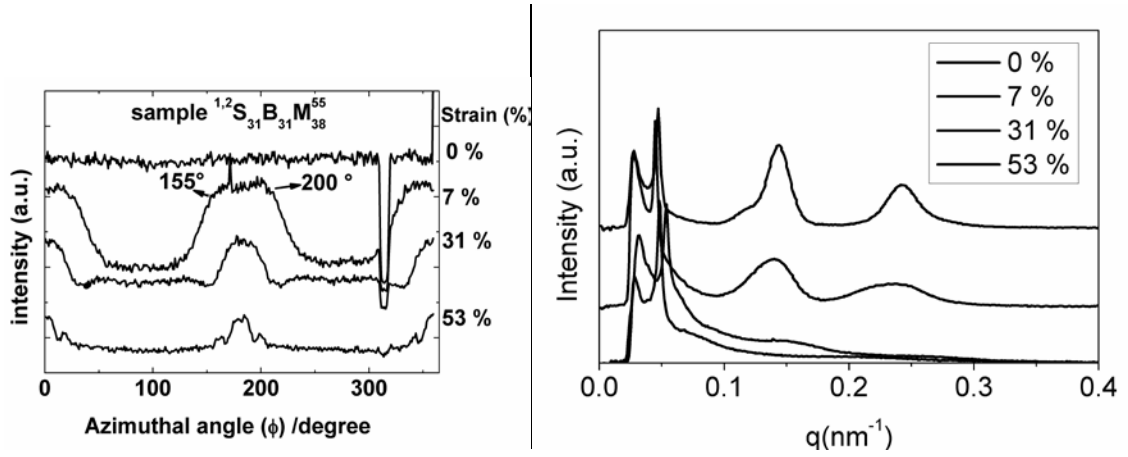

a) b)

Figure 6: *Results of the combination of SAXS and tensile testing for* $^{1,2}S_{31}B_{31}M_{38}^{55}$. *a)Plot of the azimuthal angle versus the diffusion intensity at q = 0.14 nm*$^{-1}$. *b) 1D-SAXS scattering profiles for ε = 0%, ε =7%, ε =31%, and ε = 53%*

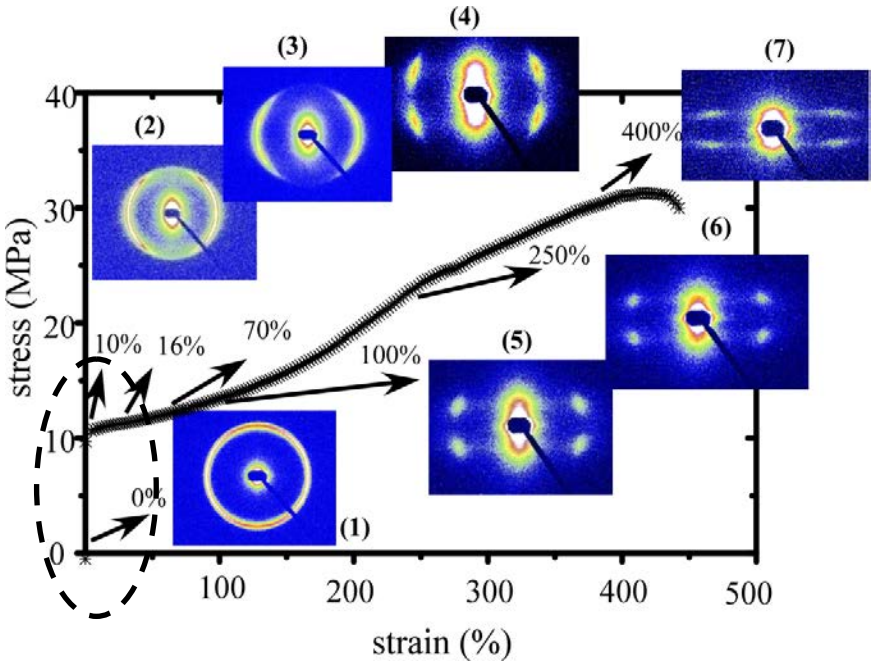

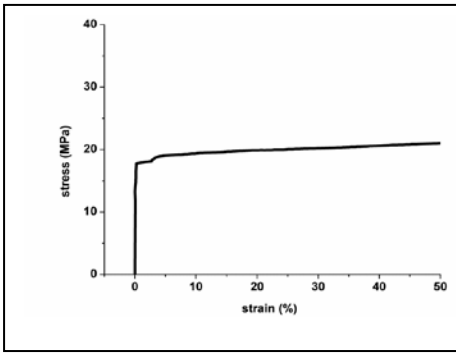

Figure7: *Results of the combination of SAXS and tensile testing for* $^{1,4}S_{30}B_{29}M_{41}{}^{53}$. *Stress-strain diagram with the 2D-SAXS patterns obtained at strain of (1)* $\varepsilon = 0$ *%, (2)* $\varepsilon = 10$ *%, (3)* $\varepsilon = 16\%$, *(4)* $\varepsilon = 70\%$, *(5)* $\varepsilon = 100\%$, *(6)* $\varepsilon = 250$ *%, and (7)* $\varepsilon = 400$ *%*

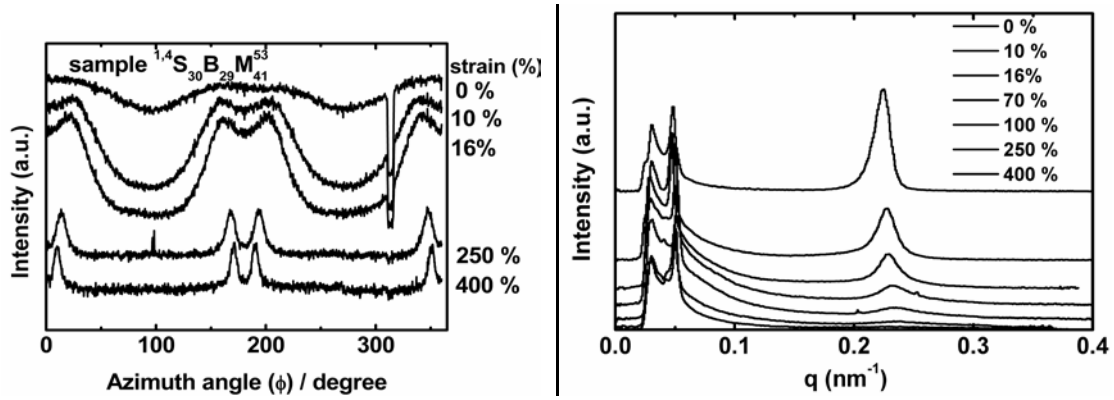

a) b)

Figure 8: *Results of the combination of SAXS and tensile testing for* $^{1,4}S_{30}B_{29}M_{41}{}^{53}$. *a) Plot of the azimuthal angle versus the scattering intensity for the first order reflection,b) 1D-SAXS scattering profiles for (top to bottom)* $\varepsilon = 0$ *%,* $\varepsilon = 10$ *%,* $\varepsilon = 16\%$, $\varepsilon = 70\%$, $\varepsilon = 100\%$, $\varepsilon = 250$ *%, and* $\varepsilon = 400$ *%*

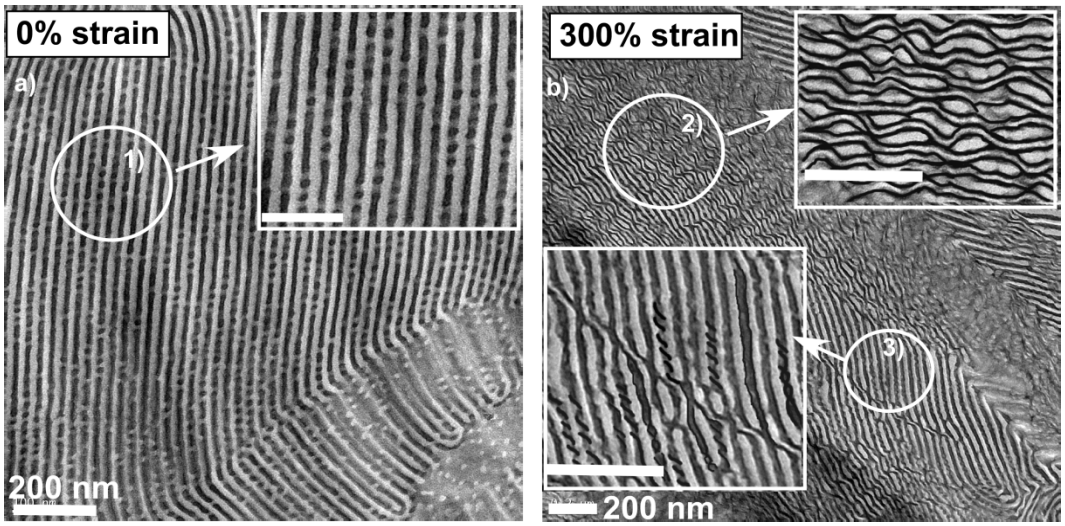

Figure 9: *TEM micrographs of* $^{1,2}S_{32}B_{31}M_{37}^{91}$ *a)* $\varepsilon = 0\%$ *highlighting lamellar phases of different domains. In parts (cf. circle and magnification) the B phase arranges in cylinders which are disconnected from the lamellar domains.*

b) $\varepsilon = 300\%$ *with wavy and twisted B domains are observed (contrast enhanced for to improve the visibility)*

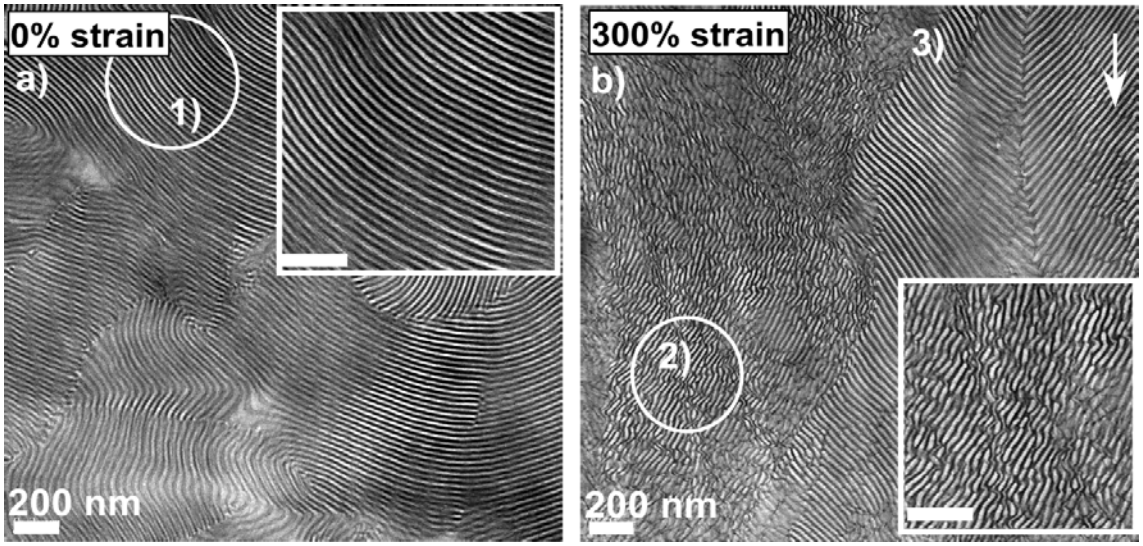

Figure 10: *TEM micrographs of* $^{1,4}S_{34}B_{31}M_{35}^{80}$

a) $\varepsilon = 0\%$ *well segregated lamellae (cf. circle and magnification)*

b) $\varepsilon = 300\%$*, a zig-zag lamellar pattern (white arrow indicates stretching direction). In parts highly undulated lamellar are observed (cf. circle 2 and the magnification)*

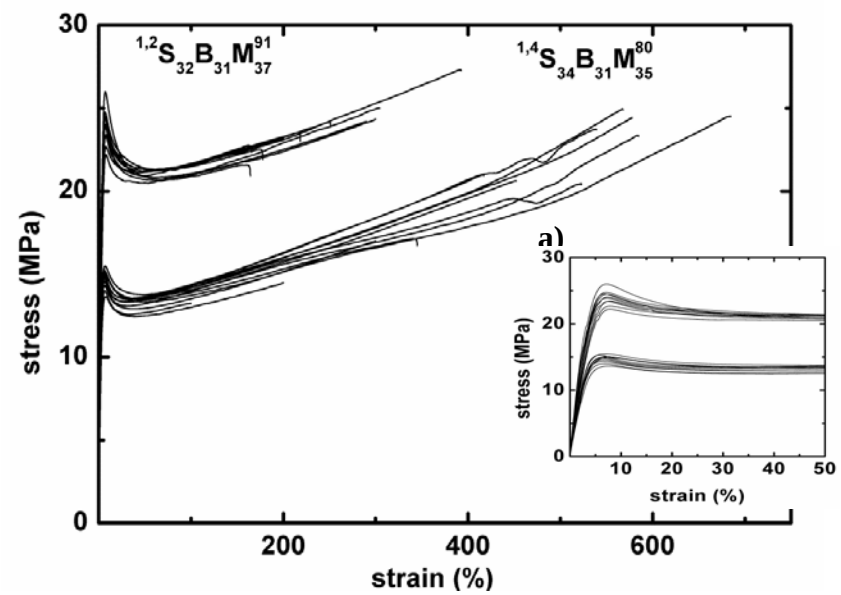

Figure 11: *Stress-strain curve of several specimens of the ternary triblockterpolymers* $^{1,2}S_{32}B_{31}M_{37}^{91}$ *and* $^{1,4}S_{34}B_{31}M_{35}^{80}$*. Magnification for strains ε< 50 % is shown inside the plot*

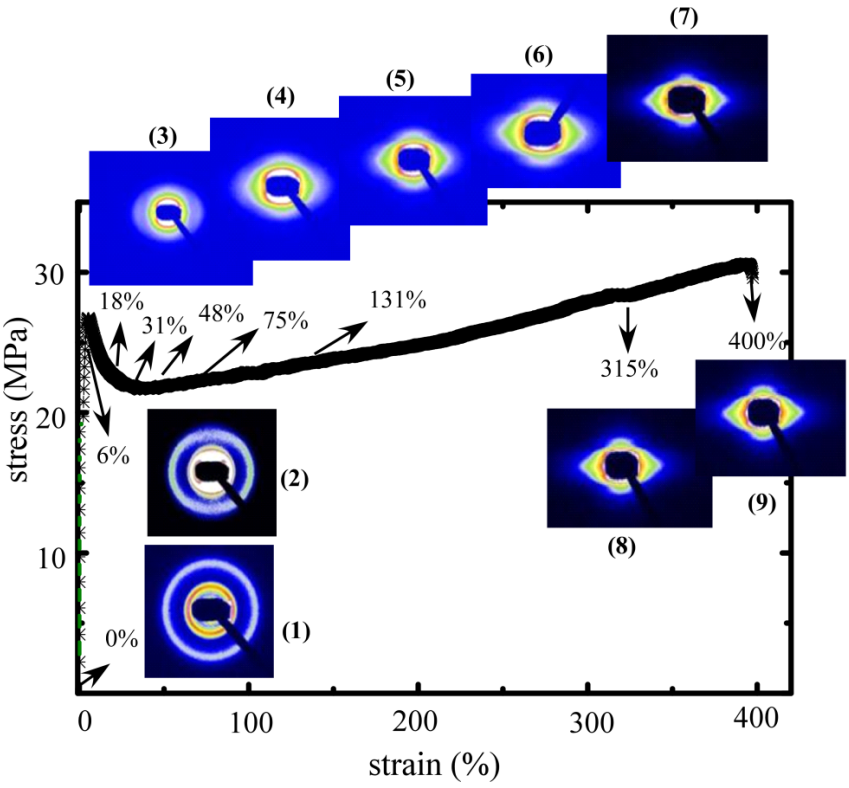

Figure 12: *Results of the combination of SAXS and tensile testing for* $^{1,2}S_{32}B_{31}M_{37}^{91}$. *Stress-strain diagram with the 2D-SAXS patterns at (1) ε = 0 %, (2) ε =6 %, (3) ε = 18%, (4) ε = 31%, (5) ε = 48 %, (6) ε = 75 %, (7) ε = 131%, (8) ε = 315 %, and (9) ε = 400 %.*

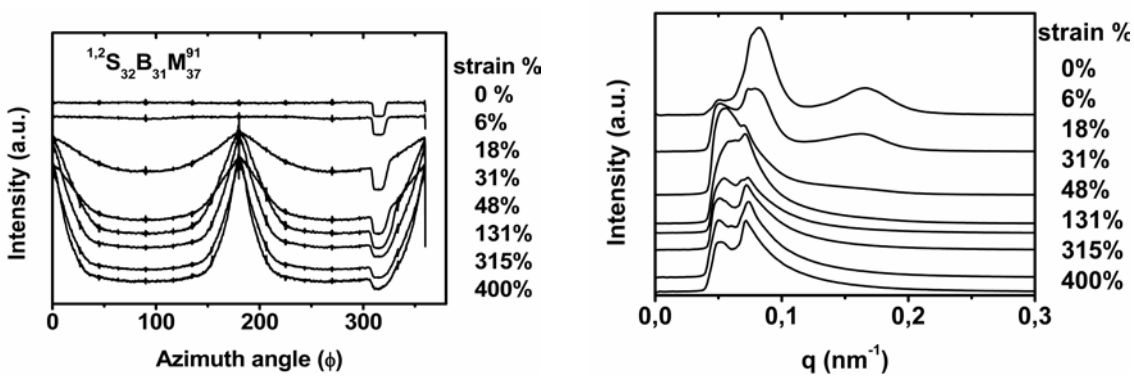

a) b)

Figure 13: *Results of the combination of SAXS and tensile testing for* $^{1,2}S_{32}B_{31}M_{37}^{91}$ *for ε = 0 %, ε =6 %, ε = 18%, ε = 31%, ε = 48 % , ε = 131 %,ε = 315 %, and ε = 400 % (from top to bottom), a) Azimuthal scattering intensity at q = 0.16 nm*$^{-1}$*, b) 1D-SAXS scattering profiles*

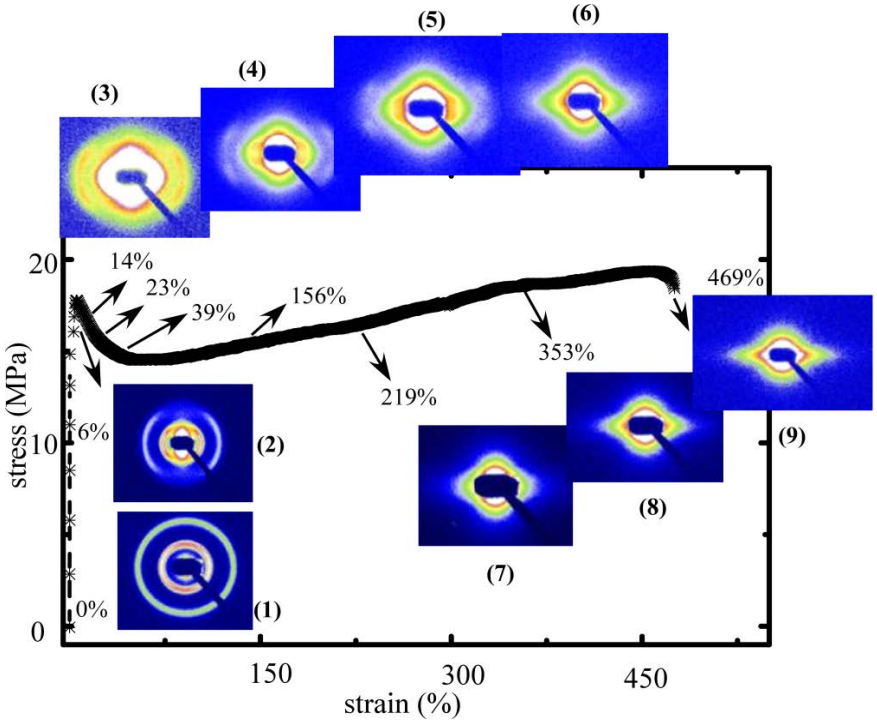

Figure 14: *Results of the combination of SAXS and tensile testing for* $^{1,4}S_{34}B_{31}M_{35}^{80}$. *Stress-strain diagram with the 2D-SAXS patterns obtained at (1) ε = 0 %, (2) ε =6 %, (3) ε = 14%, (4) ε = 23%, (5) ε = 39 %, (6) ε = 156 %, (7) ε = 219 %, (8) ε = 353 %, and (9) ε = 469 %*

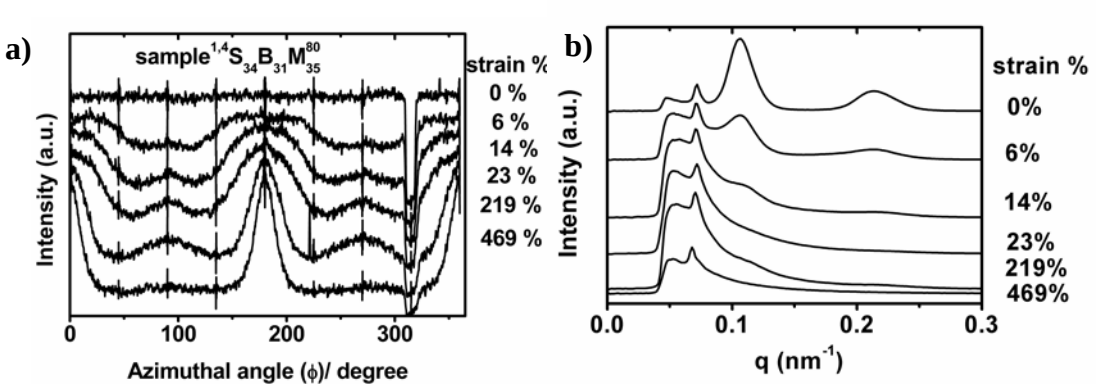

Figure 15: *Results of the combination of SAXS and tensile testing for* $^{1,4}S_{34}B_{31}M_{35}^{80}$ *for ε = 0 %, ε =6 %, ε = 14%, ε = 23%, ε = 219 %, and ε = 469 % (from top to bottom), a) Azimuthal scattering intensity at q = 0.11 nm^{-1}, b) 1D-SAXS scattering profiles*

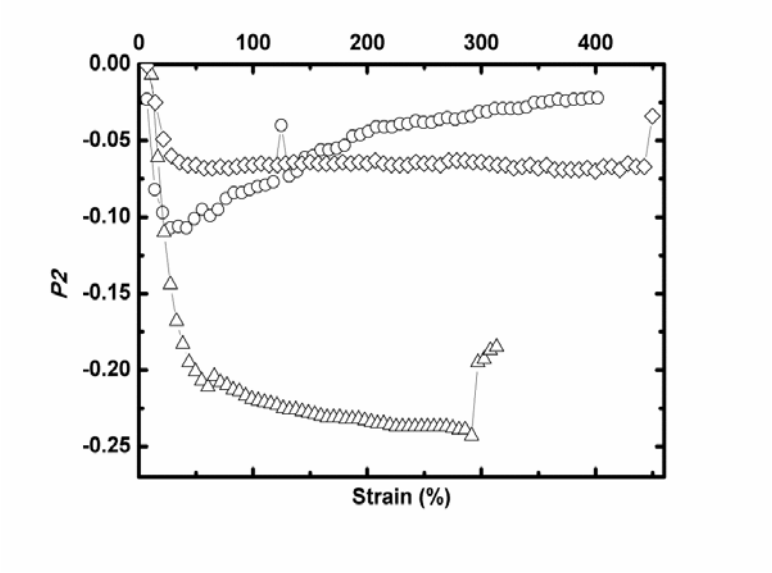

Figure 16: *Dependence of the orientation order parameter P_2 on the strain for:(Δ)$^{1,2}S_{32}B_{31}M_{37}^{91}$, (◇):$^{1,4}S_{34}B_{31}M_{35}^{80}$,and (○):$^{1,4}S_{30}B_{29}M_{41}^{53}$. Note that the orientation order parameter of $^{1,2}S_{31}B_{31}M_{38}^{55}$is not visible in the plot due to its low deformation at break*

Table 1: *Molceular characteristics of the SBM triblock terpolymers*

Triblock terpolymer		Composition (wt %)			Microstructure(%)		polydispersity
		S	B	M	*x*(1,2-B)	*x*(1,4-B)	
set 1	$S_{31}B_{31}M_{38}^{55}$	31	31	38	90	10	1.02
	$S_{30}B_{29}M_{41}^{53}$	30	29	41	16	84	1.06
set 2	$S_{34}B_{31}M_{35}^{80}$	34	31	35	18	82	1.19
	$S_{32}B_{31}M_{37}^{91}$	32	31	37	89	11	1.61

Table 2: *Mechanical properties and their standard deviation of the SBM triblock terpolymers*

Sample	**Elastic modules (E), MPa**	**yield stress σ_y(MPa)**	**yield strain ε_y (%)**	**stress at break σ_B (MPa)**	**strain at break ε_B (%)**
$^{1,2}S_{31}B_{31}M_{38}^{55}$	527±64	24±3	7±0.9	20±6	96±22
$^{1,4}S_{30}B_{29}M_{41}^{53}$	230±14	-	-	23±4	600±100
$^{1,2}S_{34}B_{31}M_{35}^{80}$	697±30	26±0.5	7±0.3	23±1	230±45
$^{1,4}S_{32}B_{31}M_{37}^{91}$	460±28	17±0.4	7±0.5	22±3	546±28

Table 3: *Glass transition temperature (T_g) of different domains of the SBM triblock terpolymers. The values obtained from DSC at 20K/min 2nd heating rate*

Sample	**PS (°C)**	**PB (°C)**	**PMMA (°C)**
$^{1,2}S_{31}B_{31}M_{38}^{55}$	94	-11	124
$^{1,4}S_{30}B_{29}M_{41}^{53}$	-	-86	123 (mixed S/M lamellae)
$^{1,4}S_{34}B_{31}M_{35}^{80}$	98	-87	119
$^{1,2}S_{32}B_{31}M_{37}^{91}$	100	-13	128

Table 3: *Domain sizes of the different lamellar domains and the long periodicity of* $^{1,4}S_{30}B_{29}M_{41}^{53}$ *after application of strain calculated from TEM micrographs and SAXS data (cf. Figure 2 and Figure 7b)*

strain (%)	**TEM**			**SAXS**
	S /M (nm)	**B (nm)**	**long period (nm)**	
0 %	8.4 ± 1.0	7.0 ± 1.0	33.3 ± 1.5	27.3
300 %	7.5 ± 1.0	5.6 ± 0.4	30.2 ± 1.0	25.1

Table 4: *Domain sizes of the different lamellar domains and the long periodicity of* $^{1,2}S_{32}B_{31}M_{37}^{91}$ *after application of strain calculated from TEM micrographs and SAXS data (cf. Figure 8 and Figure 12b)*

strain (%)	**TEM**				**SAXS**
	S (nm)	**B (nm)**	**M (nm)**	**long period (nm)**	
0 %	17± 1.0	14± 1.0	18± 2.0	65±3.0	78
300 %	15± 1.0	9± 1.0	17± 1.0	58±2.0	86

Table 5: *Domain sizes of the different lamellar domains and the long periodicity of* $^{1,4}S_{34}B_{31}M_{35}^{80}$ *after application of strain calculated from TEM micrographs and SAXS data (cf. Figure 9 and Figure 14b)*

strain (%)	**TEM**	**SAXS**

	S (nm)	B (nm)	M(nm)	long period (nm)	
0 %	16.4 ± 2.0	13.6 ± 1.0	19.2 ± 1.0	54±3	59,8
300 %	15.3 ± 1.0	10.4 ± 1.0	17.1 ± 1.0	46±3	56,1

References

1. Müller A. H. E and Matyjaszewski K. Controlled and Living Polymerizations: Wiley-VCH Verlag GmbH & Co. KGaA, 2009. pp. 493-554.
2. Abetz V and Simon P. F. W. Adv. Polym. Sci. 2005;189:125-212.
3. Huy T. A, Adhikari R, and Michler G. H. Polymer 2003;44:1247-1257.
4. Adhikari R, Huy T.A, Henning S, Michler G.H, and Knoll K. Colloid Polym.Sci. 2004;282:1381-1391.
5. Cohen Y, Albalak R.J, Dair B.J, Capel M.S, and Thomas E.L. Macromolecules 2000;33:6502-6516.
6. Weidisch R, Ensslen M, Michler G.H, and Fischer H. Macromolecules 1999;32:5375-5382.
7. Adhikari R and Michler G. H. Prog. Polym. Sci. 2004;29:949-986.
8. Pakula T, Saijo K, Kawai H, and Hashimoto T. Macromolecules 1985;18:1294-1302.
9. Fujimura M, Hashimoto T, and Kawai H. Rubber Chem. Technol. 1978;51:215-224.
10. Yamaoka I and Kimura M. Polymer 1993;34:4399-4409.
11. Odell J.A and Keller A. Polym. Eng. Sci. 1977;17:544-559.
12. Kawai H, Hashimoto T, Miyoshi K, Uno H, and Fujimura M. J. Macromol. Sci. Phys. 1980;B17(3):427-472.
13. Adhikari R, Michler G.H, Henning S, Godehardt R, Huy T.A, Goerlitz S, and Knoll K. J. App. Polym. Sci 2004;92:1219-1230.

14. Adhikari R, Godehardt R, Lebek W, Weidisch R, Michler G.H, and Knoll K. J. Macromol. Sci. Phys. 2001;B40(5):833-847.
15. Brinkmann-Rengel S, Abetz V, Stadler R, and Thomas E.L. Kautschuk Gummi Kunststoffe 1999;12:806-813.
16. Weidisch R, Goerlitz S, Michler G.H, and Stadler R. 10th Int. Conf. Deformation, Yield and Fracture of Polymers. Cambridge, UK, 1997.
17. Brinkmann Rengel S. Thermoplastic Elastomere auf Basis von ABA und ABC Dreiblockcopolymer. Fachbereich Chemie und Pharmazie, vol. PhD thesis: Johannes Gutenberg-Universität Mainz, 1998.
18. Auschra C and Stadler R. Polymer Bull. 1993;30:257-264.
19. http://www.esrf.eu/computing/scientific/FIT2D/.
20. Michler G.H, Adhikari R, Lebek W, Goerlitz S, Weidisch R, and Knoll K. J. App. Polym. Sci. 2002;85:683-700.
21. Seguela R and Prud'homme J. Macromolecules 1981;14:197-202.
22. Honeker C.C and Thomas E.L. Chem. Mater. 1996;8:1702-1714.
23. Schwier C.E, Argon A.S, and Cohen R.E. Polymer 1985;26:1985-1993.
24. Meijer H.E.H and Govaert L.E. Prog. Polym.Sci. 2005;30:915-938.
25. Kierkels J.T.A. Tailoring the mechanical properties of amorphous polymers. vol. Proefschrift: Technische Universiteit Eindhoven, 2006.
26. Adhikari R, Michler G.H, Lebek W, Goerlitz S, Weidisch R, and Knoll K. J. App. Polym. Sci. 2002;85:701-713.
27. Jansen B.J.P, Rastogi S, Meijer H.E.H, and Lemstra P.J. Macromolecules 2001;34:4007-4018.
28. Böker A, Elbs H, Hänsel H, Knoll A, Ludwings S, Zettl H, Zvelindovsky A.V, Sevink G. J. A, Urban V, Abetz V, Müller A.H.E, and Krausch G. Macromolecules 2003;36:8078-8087.